Undrained Stability of Footings on Slopes

J. S. Shiau[1]; R. S. Merifield[2]; A. V. Lyamin[3]; and S. W. Sloan[4]

Abstract: Solutions for the ultimate bearing capacity of footings on purely cohesive slopes are obtained by applying finite element upper and lower bound methods. In a footing-on-slope system, the ultimate bearing capacity of the footing may be governed by either foundation failure or global slope failure. The combination of these two factors makes the problem difficult to solve using traditional methods. The importance of a dimensionless strength ratio in determining the footing capacity is broadly discussed, and design charts are presented for a wide range of parameters. In addition, the effect of footing roughness and surface surcharge are briefly quantified. **DOI: 10.1061/(ASCE)GM.1943-5622.0000092.**

CE Database subject headings: Footings; Limit states; Load bearing capacity; Slope stability; Finite element method.

Author keywords: Limit analysis; Bearing capacity; Slope stability; Finite elements; Nonlinear programming.

Introduction

A number of engineering structures require foundation systems to be placed near an existing slope. Such structures include bridge abutments and tower footings for electrical transmission lines (Shields et al. 1990). It is also often the case that foundations are placed near a proposed excavation for the basement construction of high-rise buildings in urban areas.

For a footing-on-slope system, the ultimate bearing capacity of the footing may be governed by either the foundation bearing capacity or the overall stability of the slope. The combination of these two factors makes the problem difficult to solve. A variety of methods has been proposed, including slip-line methods (Sokolovski 1960), limit equilibrium techniques (Meyerhof 1957; Narita et al. 1990) and yield design theory (de Buhan and Garnier 1994, 1998). Upper and lower bounds to this problem have been derived analytically by Davis and Booker (1973), whereas analytical upper bound solutions have been presented by Kusakabe et al. (1981). Although slip-line analyses have the advantage that they are mathematically rigorous, they are difficult to apply, especially for problems with complex geometries or complicated loading. Limit equilibrium methods, on the other hand, although less rigorous than slip-line methods, can be generalized to deal with a variety of complicated boundary conditions, soil properties, and loading conditions. Although the accuracy of limit equilibrium solutions is sometimes questionable, this approach is often favored in design practice because of its simplicity and generality.

[1]Senior Lecturer, Faculty of Engineering and Surveying, Univ. of Southern Queensland, QLD 4350, Australia (corresponding author). E-mail: jimshiau@usq.edu.au

[2]Senior Lecturer, Center for Geotechnical and Materials Modelling, The Univ. of Newcastle, NSW 2308, Australia.

[3]Associate Professor, Center for Geotechnical and Materials Modelling, The Univ. of Newcastle, NSW 2308, Australia.

[4]Professor, Center for Geotechnical and Materials Modelling, The Univ. of Newcastle, NSW 2308, Australia.

Note. This manuscript was submitted on March 1, 2010; approved on September 8, 2010; published online on September 15, 2011. Discussion period open until March 1, 2012; separate discussions must be submitted for individual papers. This paper is part of the ***International Journal of Geomechanics***, Vol. 11, No. 5, October 1, 2011. ©ASCE, ISSN 1532-3641/2011/5-381–390/$25.00.

Another approach for analyzing the stability of geotechnical structures is to use the lower and upper bound limit theorems developed by Drucker et al. (1952). These theorems are based on statically admissible stress fields and kinematically admissible velocity fields, respectively, and can be used to bracket the exact ultimate load from below and above. The limit theorems are most powerful when both types of solutions can be used to bracket the true limit load to within a few percent from above and below. However, this accuracy is seldom possible to achieve by using analytical upper and lower bound formulations. Most applications of the limit theorems are based on the upper bound theorem alone (e.g., Chen 1975; Michalowski 1995). This is because it is usually simpler to postulate a good kinematically admissible failure mechanism than to construct a good statically admissible stress field.

Over the last two decades Sloan (1988, 1989), Sloan and Kleeman (1995) and Lyamin and Sloan (2002a, b) introduced finite-element limit analysis formulations that permit large two-dimensional problems to be solved efficiently on a standard personal computer. Estimates of the ultimate bearing capacity herein have been obtained by using the latest versions of these procedures proposed by Lyamin and Sloan (2002a, b) and Krabbenhøft et al. (2005). Full details of the formulations can be found in the relevant references and will not be discussed here.

Problem Definition

The bearing capacity problem of a rigid foundation resting near a slope is illustrated in Fig. 1. A strip footing of width B is located on a homogeneous clay soil with a slope angle β and slope height H at a distance L from the edge of the slope. The soil behavior is assumed to be undrained following the Tresca yield criterion with a shear strength $c_u(\Phi_u = 0)$. Note that such an assumption may result in an overestimation of the problem. This is because, in practice, tension cracks are often observed in the field.

The limit behavior of such a rigid foundation system is influenced by the slope angle β and the distance L. The ultimate bearing capacity will also depend on the soil unit weight γ that affects the overall stability of the slope. This is different from the undrained bearing capacity of a surface footing resting on level ground in which the ultimate bearing capacity is independent of the soil unit weight. The ultimate bearing capacity for the problem considered can then be stated as

$$\frac{p}{\gamma B} = f\left(\beta, \frac{L}{B}, \frac{c_u}{\gamma B}, \frac{q}{\gamma B}, \frac{H}{B}\right) \quad (1)$$

in which p = the average limit pressure acting on the footing and q = the surcharge load as shown in Fig. 1. Accordingly, the bearing capacities are presented in the dimensionless quantities β, L/B, and $c_u/\gamma B$, with the role of the footing roughness and slope surcharge $(q/\gamma B)$ investigated separately. H/B is equal to three in all analyses, which causes *above the toe* failure that is covered in this paper.

A typical lower bound finite element mesh for the problem of a rigid footing resting near a slope surface is shown in Fig. 2. The mesh consists of 1,605 elements with a total of 4,815 nodes and 2,364 discontinuities. In the lower bound calculation, a discontinuity in the tangential stress may occur across all shared element edges. If n and t denote the normal and the tangent directions to the discontinuity, σ_n is the only stress component that may be discontinuous. Unlike meshes in the displacement finite-element method, the lower bound mesh discretization permits several nodes to share the same coordinates. This extra degree of freedom, although increasing the total number of the problem variables, improves the solution accuracy. Note that extension elements can also be used to extend the stress field throughout the semiinfinite domain (Lyamin 1999). The unknown stress field is then sought that maximizes an integral of the normal pressure over some part of the boundary (see Fig. 2).

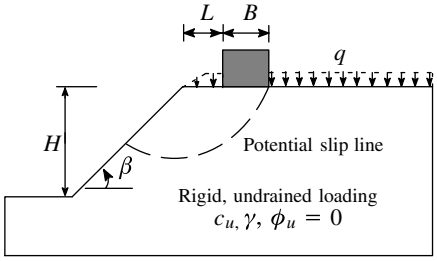

Fig. 1. Problem notation and potential failure mechanism

For both the upper and lower bound computations, a zero thickness interface (discontinuity) is introduced between the footing (which is modeled as a rigid block) and the soil. Each discontinuity element is actually comprised of two triangular solid elements with the end nodes collapsed to a single point as described in Krabbenhøft et al. (2005). For the elements, the cohesion (strength) is set as $c = 0$ for the smooth case and $c = c_u$ for the rough case. Prescribing these ensures that the shear stress underneath the footing is zero for the smooth case and not greater than c_u for the rough case.

Fig. 3 shows an example of a finite-element mesh for the upper bound limit analysis. The upper bound mesh consists of 2,140 elements with a total of 6,420 nodes and 3,160 discontinuities.

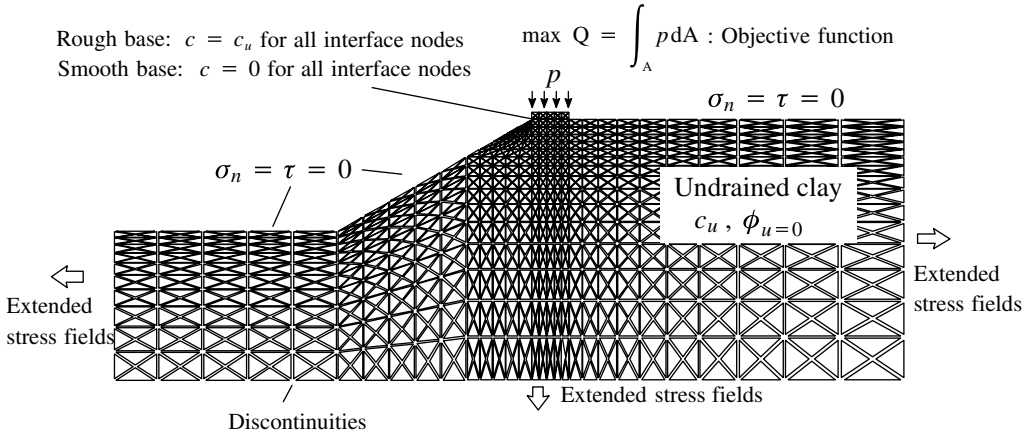

Fig. 2. Typical finite-element mesh for lower bound analysis ($\beta = 30°$, $L/B = 0$)

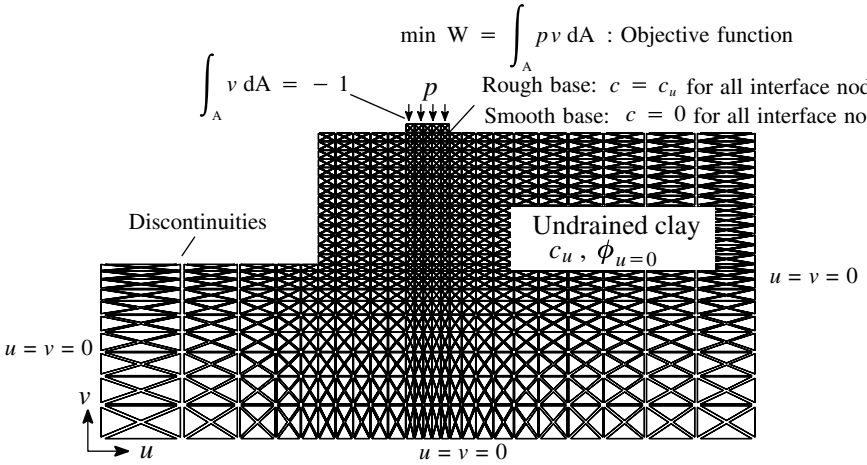

Fig. 3. Typical finite-element mesh for upper bound analysis ($\beta = 90°$, $L/B = 2$)

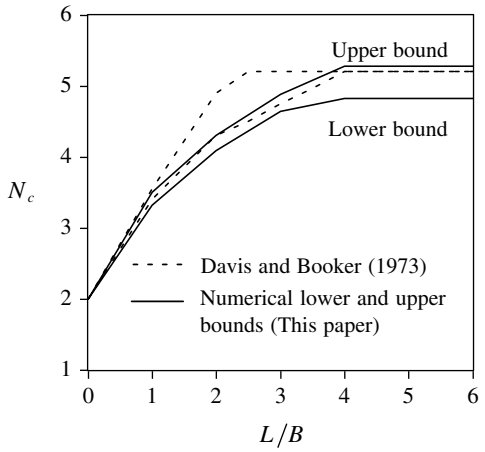

Fig. 4. Lower and upper bound bearing capacity for weightless slopes (smooth base, $\beta = 90°$)

Note that all element nodes along the footing-soil interface are not constrained and the footing is free to move horizontally, vertically, and in rotation.

An upper bound solution is obtained by minimizing the rate of internal energy dissipation less the rate of work done by the prescribed loads (i.e., soil weight and surcharge). Subject to the flow rule, boundary, and scaling constraints on the velocity field, this quantity is then equated to the rate of work done by the unknown (optimizable) loads.

Results and Discussion

By using the methods outlined previously, finite-element limit analyses were performed to obtain both lower and upper bound bearing capacity estimates for strip footings on purely cohesive slopes. The study assumes the soil obeys an associated flow rule and covers a range of parameters, including the slope angle (β), the footing distance to the crest (L/B), and the dimensionless parameter ($c_u/\gamma B$). These results, along with the effects of surcharge ($q/\gamma B$) and footing roughness are also quantified. Where possible, the new numerical results are compared to solutions obtained by others.

Weightless Slopes

For verification purposes, Fig. 4 presents the bearing capacity for various footing locations on a weightless vertical cut. Numerical upper and lower bounds are compared with those analytically derived by Davis and Booker (1973). For such a system, the undrained bearing capacity p can be simply expressed as $p = c_u N_c$ in which N_c is a dimensionless bearing capacity factor and c_u is the undrained soil strength. Interestingly, the bound results given by Davis and Booker (1973) in the range of $1 < L/B < 4$ have been greatly improved by using the finite-element bounding methods. The results for $L/B > 4$ are less accurate than those of Davis and Booker, yet could be improved with finer finite-element meshes. Our numerical results confirm that the vertical cut has no effect on the footing bearing capacity for cases with $L/B \geq 4$. Importantly, the bearing capacity is reduced by a factor of 2.5 as the footing distance ratio L/B is decreased from 4 to 0.

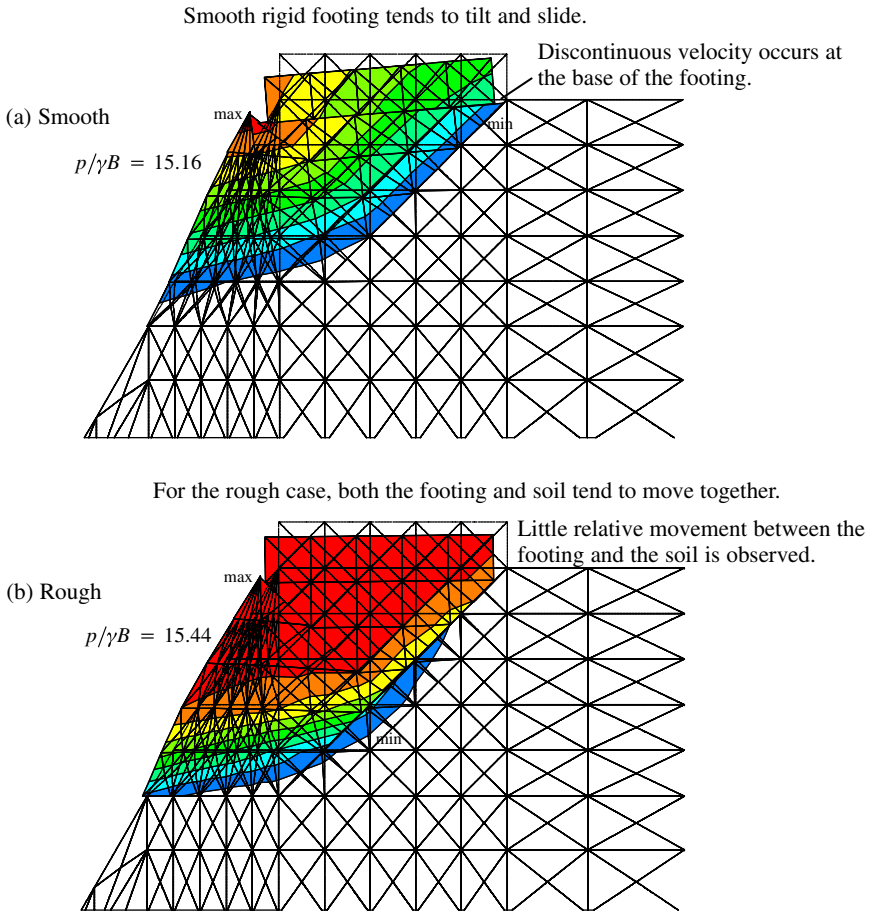

Fig. 5. Comparison of deformed shapes and velocity contours for smooth and rough footings ($\beta = 60°$, $L/B = 0$, $c_u/\gamma B = 5$)

Table 1. Upper Bound Results for Rough and Smooth Footings ($\beta = 60°$)

	$p/\gamma B$							
	$L/B = 0$		$L/B = 1$		$L/B = 2$		$L/B = 3$	
$c_u/\gamma B$	Smooth	Rough	Smooth	Rough	Smooth	Rough	Smooth	Rough
10	30.65	31.32	43.14	43.18	50.28	50.29	52.82	53.20
5	15.16	15.44	21.26	21.27	24.80	24.81	26.68	27.00
3	8.95	9.08	12.46	12.46	14.40	14.54	15.31	15.96
1	2.63	2.63	3.18	3.19	3.66	3.66	4.20	4.20

Effect of the Footing Roughness

The effect of the footing roughness may or may not be significant depending on the relative movement between the footing and the bearing soil. Fig. 5 compares deformed shapes and velocity contours for smooth and rough footings on a 60° slope ($L/B = 0$, $\beta = 60°$). Denote that (u, v) are the horizontal and vertical velocity components, and the contoured velocity field shows the resultant velocity; i.e., $\sqrt{u^2 + v^2}$. Although the precise values of the velocity contours are not important, their maximum and minimum positions are indicated in the figure. For the smooth case shown in Fig. 5(a), the rigid footing tends to tilt and slide, and a discontinuous velocity is observed at the base of the footing. In contrast, for the perfectly rough case [Fig. 5(b)], both the footing and soil displace together and little relative movement is observed at the soil/footing interface. Note that a larger failure zone is obtained for the rough case, indicating greater bearing capacity for a rough footing. Table 1 presents the upper bound results for both smooth and rough cases of a 60° slope ($\beta = 60°$). In general, rough cases produce results that are approximately 1–2% higher than those for smooth cases. For a lower strength ratio (e.g., $c_u/\gamma B = 1$), identical results for smooth and rough cases are obtained.

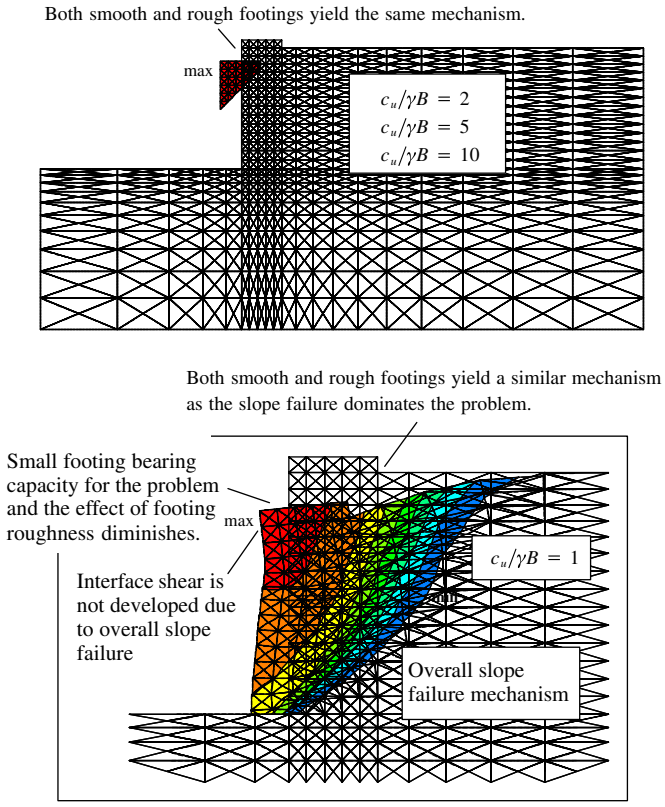

Fig. 6. Comparison of deformed shapes and velocity contours for smooth and rough footings ($\beta = 90°$, $L/B = 0$)

Fig. 6 compares deformed shapes and velocity fields for various strength ratios $c_u/\gamma B$ of a vertical slope ($L/B = 0$, $\beta = 90°$). For stronger slopes ($c_u/\gamma B \geq 2$), the failure mechanism consists of a rigid triangular wedge. Note that both the soil and the footing move sideways together and an interface shear is not developed. This indicates that the bearing capacity for both rough and smooth cases should be identical, which is confirmed in Table 2. For a lower strength ratio (e.g., $c_u/\gamma B = 1$), overall slope failure dominates the problem, and the effect of footing roughness is minimal because the footing is free to move laterally. Table 2 shows the upper bound results for both smooth and rough cases of a vertical slope ($\beta = 90°$). In general, identical smooth and rough results are obtained for cases with $L/B = 0$. For $L/B > 1$, the rough cases produce slightly higher results than those obtained for smooth cases.

In practice, the true footing roughness is likely to lie somewhere between the perfectly smooth and perfectly rough extremes. It is normally conservative to adopt the bearing capacity of smooth footings in design practice (Shiau et al. 2003). In the following sections, numerical results are presented for smooth footings.

Effect of the Dimensionless Strength Ratio $c_u/\gamma B$

For slopes with unit weight γ, a dimensionless strength ratio can be defined as $c_u/\gamma B$, and a normalized bearing capacity will be presented as $p/\gamma B$ for both upper and lower bounds. Unlike the bearing capacity for level ground, the unit weight γ plays an important role in the footing-on-slope problem.

Table 2. Upper Bound Results for Rough and Smooth Footings ($\beta = 90°$)

	$p/\gamma B$							
	$L/B = 0$		$L/B = 1$		$L/B = 2$		$L/B = 3$	
$c_u/\gamma B$	Smooth	Rough	Smooth	Rough	Smooth	Rough	Smooth	Rough
10	19.95	19.95	33.75	33.79	41.31	41.33	47.30	47.32
5	9.50	9.50	16.12	16.17	19.64	19.65	22.73	22.74
3	5.50	5.50	9.01	9.01	10.85	10.88	12.72	12.78
1	1.32	1.32	1.20	1.20	1.46	1.46	1.99	1.99

Fig. 7 presents typical upper and lower bound results for a vertical slope ($c_u/\gamma B = 5$). In general, numerical upper and lower bounds obtained for slopes over a range of $c_u/\gamma B$ values were found to bracket the true estimates within 3.86% [$100(UB - LB)/(2LB) = 100(26.39 - 24.50)/(2 \times 24.50)$]. Note that better accuracy was obtained at small L/B ratios. As a consequence, an average value of the upper and lower bound bearing capacity $p/\gamma B$ has been calculated and will be used for the following discussions.

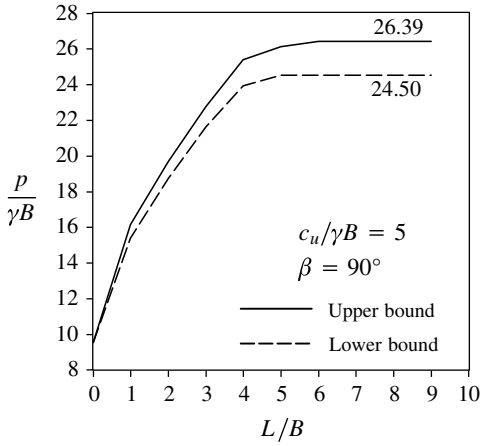

Fig. 7. Typical upper and lower bound results ($c_u/\gamma B = 5$, $\beta = 90°$, smooth base)

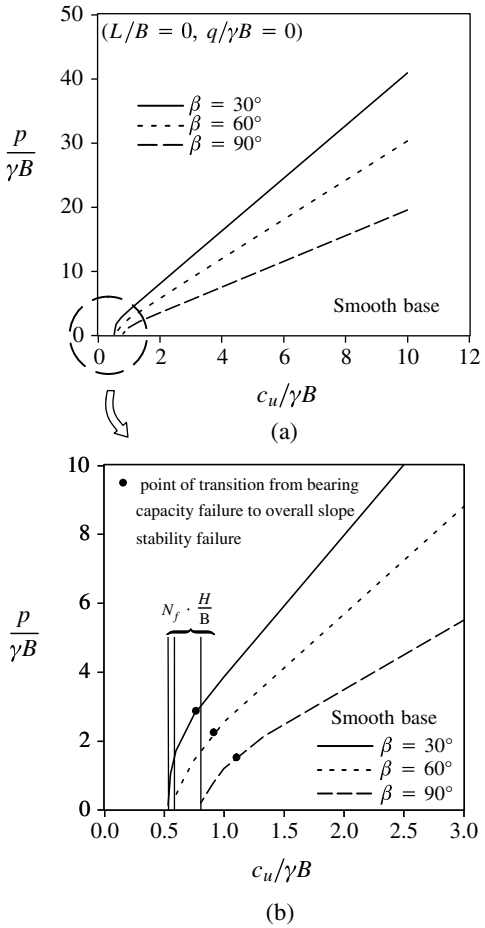

Fig. 8. Averaged upper and lower bounds for various slope angles

The average upper and lower bound estimates of the normalized bearing capacity $p/\gamma B$ are presented in Figs. 8–11 for L/B ranging from 0 to 6 and $c_u/\gamma B$ up to 10. Note that the dimensionless bearing capacity $p/\gamma B$ decreases linearly with the strength ratio ($c_u/\gamma B$) until it becomes nonlinear and rapidly approaches 0 at a particular value of $c_u/\gamma B$ in which no feasible solution is available from the numerical analysis. This is a feature common to all the results shown in Figs. 8–11 and is worth discussing in more detail.

The linear portion of the curves shown in Figs. 8–11 indicate bearing capacity failures that are contained within the face of the slope, so the ratio H/B has no influence. Some of these failure mechanisms are shown in Figs. 12 and 13.

The nonlinear curves shown on the plots in Figs. 8–11 reflect the complex interaction between the footing bearing capacity, and the overall slope stability and can be best explained by referring to the magnified zone shown in Fig. 8(b). The point at which the curve begins to become nonlinear is highlighted in this figure. These three points mark the transition from bearing capacity failure to overall slope stability failure where $p/\gamma B = 0$. This transition can be readily observed in Fig. 14, which shows the velocity contours for various values of $c_u/\gamma B$. Interestingly, the slip surfaces for the weightless slope and slopes with $c_u/\gamma B \geq 0.750$ [Fig. 14(a)] are very similar and confined to a bearing failure mechanism. As the value of $c_u/\gamma B$ decreases, the failure mechanisms transform from a bearing capacity failure (face failure) to a complete slope failure at $c_u/\gamma B = 0.556$ [Fig. 14(d)]. Also note that the assumption of *above the toe* failure analysis is not strictly valid for cases with small values of strength ratio, such as $c_u/\gamma B = 0.60$ in Fig. 14. For *below the toe* failure analysis, a value of H/B (slope height ratio) needs to be considered in the analysis.

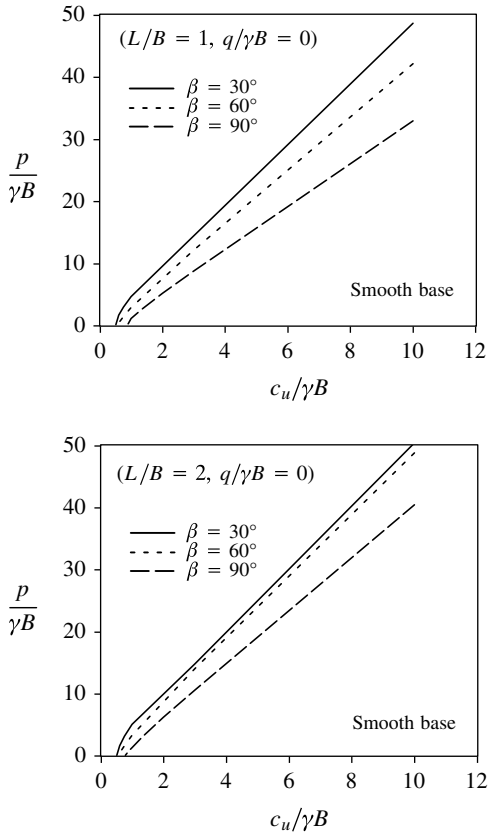

Fig. 9. Averaged upper and lower bounds for various slope angles

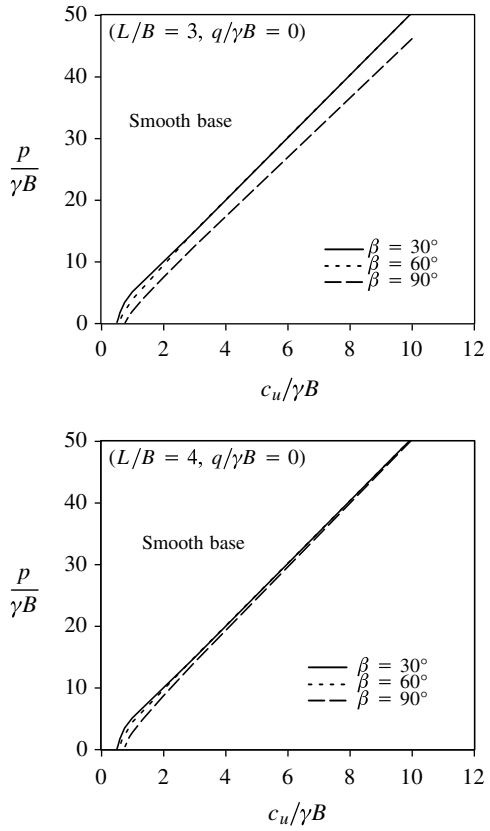

Fig. 10. Averaged upper and lower bounds for various slope angles

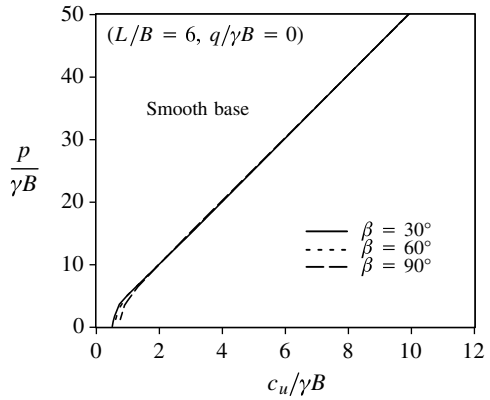

Fig. 11. Averaged upper and lower bounds for various slope angles

With reference to Fig. 8(b), another point worth noting is the value of $c_u/\gamma B$, which corresponds to a normalized bearing capacity of zero ($p/\gamma B = 0$) (i.e., where the curves cross the x-axis). To determine this value, it is first worth discussing the stability of slopes in general, without a footing on the crest.

By using the finite-element bounds, the average critical overburden factor $(\gamma H/c_u)_{\text{critical}}$ for slopes with $\beta = 30°$, 60°, and 90° were found to be 5.61, 5.10, and 3.72 from a self-weight induced failure assuming a rigid base at infinite depth, respectively. This critical value of $\gamma H/c_u$ can be converted to a stability number that is defined as $N_f = c_u/\gamma H F_s$ in which F_s is the factor of safety. For a factor of safety of one, the preceding finite-element values of $(\gamma H/c_u)_{\text{critical}}$ indicate stability numbers of $N_f = 0.178$, 0.196, and 0.269 for $\beta = 30°$, 60°, and 90°, respectively. By looking at

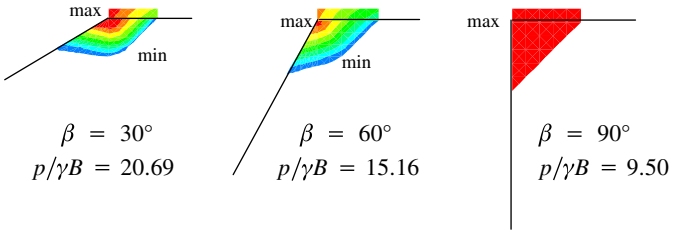

Fig. 12. Velocity contours for various slope angles ($c_u/\gamma B = 5$, $L/B = 0$, smooth base)

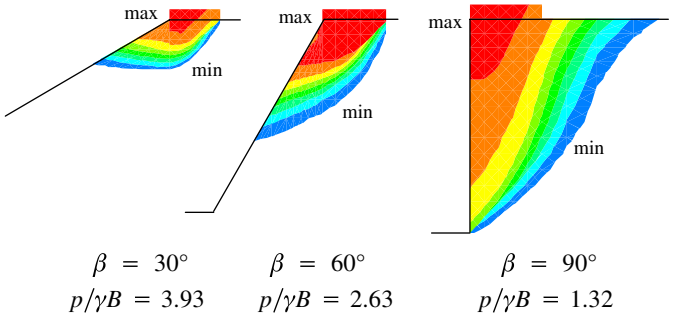

Fig. 13. Velocity contours for various slope angles ($c_u/\gamma B = 1$, $L/B = 0$, smooth base)

the key dimensionless variables, we can relate the stability number to the dimensionless parameter $c_u/\gamma B$ as follows:

$$N_f \frac{H}{B} = \frac{c_u}{\gamma H F_s}\frac{H}{B} = \frac{c_u}{\gamma B} \quad \text{for} \quad F_s = 1.0 \tag{2}$$

Eq. (2) indicates that the normalized bearing capacity $p/\gamma B$ will be 0 (i.e., the curves will cross the x-axis) at values of $(c_u/\gamma B)_{\text{crit}}$ equal to $N_f H/B$. This point corresponds to overall slope stability failure. As mentioned previously, the analyses shown in Fig. 8(b) were for $H/B = 3$. Therefore, on the basis of the preceding discussions and Eq. (2), $p/\gamma B$ will be zero at $(c_u/\gamma B)_{\text{crit}} = 0.535$, 0.588, and 0.807 for $\beta = 30°$, 60°, and 90°, respectively. This is confirmed in Fig. 8(b) in which these values are shown graphically as vertical lines. The stability charts, such as those presented by Taylor (1937) or the more rigorous solutions of Chen (1975), can also be used in conjunction with Eq. (2) to indicate where the normalized bearing capacity $p/\gamma B$ will be zero.

From a foundation design point of view, a design engineer would be concerned with the condition of a foundation failure, and thus, knowing the critical value of strength ratio $(c_u/\gamma B)_{\text{crit}}$ for a particular slope geometry is very important. This critical value of the strength ratio distinguishes between two different failure mechanisms, namely, foundation failure $(c_u/\gamma B > (c_u/\gamma B)_{\text{crit}})$ and slope failure $(c_u/\gamma B \leq (c_u/\gamma B)_{\text{crit}})$. The design engineer would not proceed to the curved portion of the charts in Figs. 8–11 because the slope is in a marginally stable condition and the foundation loading could trigger a slope failure.

Table 3 compares the numerical bounds with the available limit equilibrium solutions of Narita et al. (1990) and the analytical upper bound solutions of Kusakabe et al. (1981). The comparison is for the case with $\beta = 30°$ and $L/B = 0$. In general, good agreements were observed from the results.

Effect of the Slope Angle β

The effect of β can be found graphically in Fig. 8(a) for $L/B = 0$. As expected, the footing capacity decreases as the slope angle β is

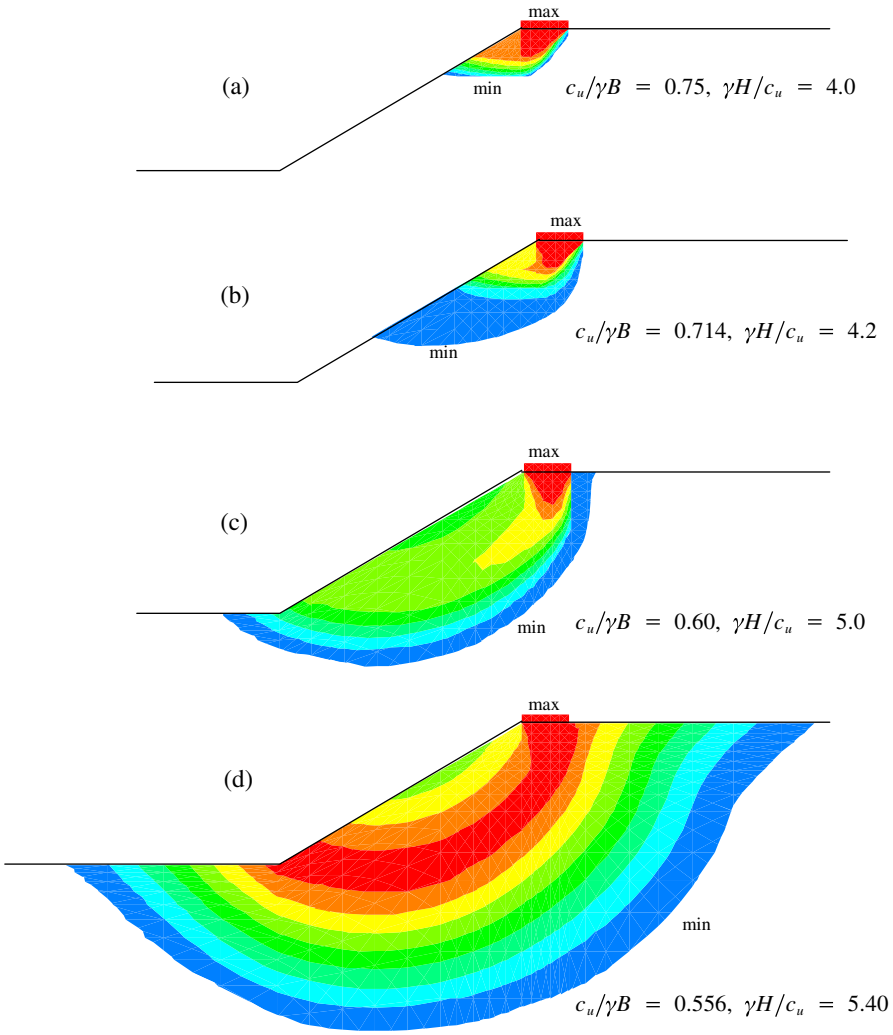

Fig. 14. Velocity contours for decreasing values of $c_u/\gamma B$ (smooth base, $\beta = 30°$, $L/B = 0$, $q/\gamma B = 0$)

Table 3. Results Comparison (Smooth Base, $\beta = 30°$, $L/B = 0$, After Narita and Yamaguchi 1990)

	$p/\gamma B$			
	Limit equilibrium	Upper bound	FE lower bound	FE upper bound
$c_u/\gamma B$	Narita and Yamaguchi(1990)	Kusakabe et al. (1981)	This paper	This paper
25	107.0	102.0	97.50	104.33
5	21.1	20.2	19.61	20.69
1	3.94	3.84	3.73	3.93
0.750	—	—	2.59	2.85
0.714	—	—	2.36	2.68
0.600	—	—	No feasible solution $p/\gamma B \to 0$	1.87
0.556	—	—	No feasible solution $p/\gamma B \to 0$	1.34

increased or the strength ratio $c_u/\gamma B$ is reduced (either a reduction in c_u or an increase in γ).

The upper bound velocity contours for various slope angles as shown in Figs. 12 and 13 in which cases with $c_u/\gamma B = 5.0$ and $c_u/\gamma B = 1.0$ are presented. For the more stable case ($c_u/\gamma B = 5.0$), the velocity fields at failure are localized for all three slope angles, resulting in the so-called face failure in the stability analysis (Fig. 12). On the other hand, for the cases with $c_u/\gamma B = 1.0$ (Fig. 13), the extent of the velocity field increases as the slope angle is increased, possibly resulting in an overall slope failure mechanism in which little bearing capacity is observed. This is certainly the case for $\beta = 60°$ and 90° and is consistent with Fig. 8(b), which indicates at a ratio of $c_u/\gamma B = 1.0$, overall slope failure is likely for these two slope angles because we are now on the curved portion of the plot.

Effect of the Footing Distance to the Crest (L/B)

Numerical lower and upper bound results on the effect of L/B are shown graphically in Fig. 15. For all values of β, the increase in footing capacity tends to stop at certain values of L/B. Fig. 15

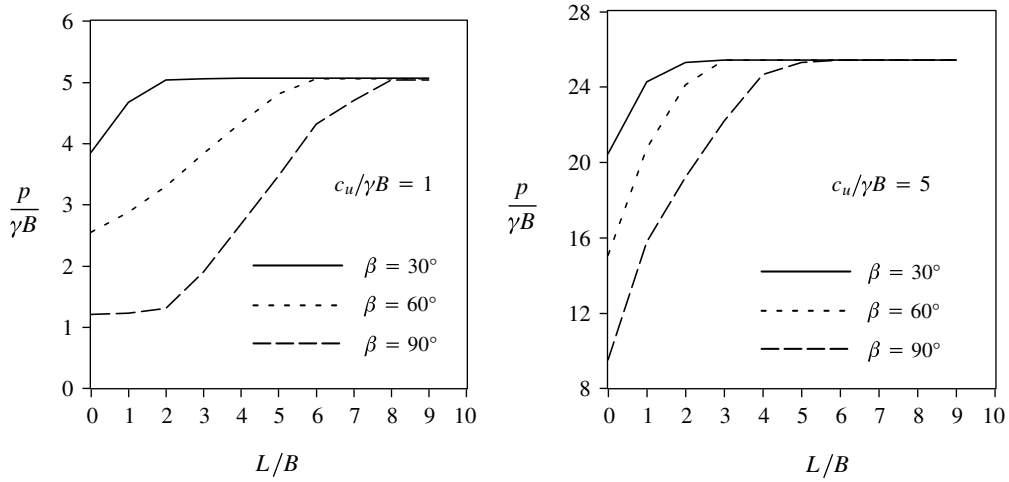

Fig. 15. Effect of L/B on the bearing capacity (smooth base)

indicates that for $c_u/\gamma B = 1.0$, $p/\gamma B$ reaches a constant value of 5.06 (which is an average of the lower and upper bounds) approximately at $L/B = 2$ for $\beta = 30°$, $L/B = 6$ for $\beta = 60°$, and $L/B = 8$ for $\beta = 90°$, respectively. On the other hand, for $c_u/\gamma B = 5.0$, $p/\gamma B$ reaches a constant value of 25.4 approximately at $L/B = 2$ for $\beta = 30°$, $L/B = 3$ for $\beta = 60°$, and $L/B = 5$ for $\beta = 90°$, respectively.

Several velocity diagrams illustrating the influence of L/B are shown in Fig. 16 for cases of a vertical cut with $c_u/\gamma B = 5.0$. This figure shows that at $L/B = 5$, the pattern of the velocity diagram is essentially identical to that for a footing placed on level ground, indicating that the vertical cut does not influence the footing performance. Interestingly, by observing the failure surfaces shown in Fig. 16, one may raise a question as to how the traditional limit equilibrium method or analytical upper bound method (both require an assumed failure mechanism) would account for these complex collapse patterns. The advantage of using finite element limit analysis in which the failure mechanism is obtained as part of the solution becomes apparent in such cases.

Effect of the Surcharge ($q/\gamma B$)

The existence of surcharge on the slope surface could either increase or decrease the footing capacity depending on both β and L/B. Figs. 17 and 18 present the averaged bounds for studying the effect of surcharge. As shown in Fig. 17 for $\beta = 30°$, an increase in $q/\gamma B$ tends to increase the footing capacity for all ratios of L/B. However, for a vertical cut ($\beta = 90°$) as shown in Fig. 18, an increase in $q/\gamma B$ will reduce the bearing capacity for all ratios of L/B, except those cases with $L/B > 5$ in which the footing is located outside the influence distance of the slope.

Fig. 19 compares the velocity diagrams for $q/\gamma B = 0$ and 1 for a 30° slope. The surcharge suppresses are shown to be the upward movement and thus, increase the footing bearing capacity. On the other hand, the existence of surcharge for cases with $L/B < 5$ for a 90° slope will have a negative effect on the slope and tend to decrease the footing bearing capacity.

Effect of H/B

As already mentioned, the results summarized in Figs. 8–11 were calculated by using a value of $H/B = 3$. To ensure that a bearing failure mechanism can develop without influence of the bottom or toe of the slope, it is important to ensure that the value of $H/B = 3$ is large enough. This can be verified by viewing all the observed

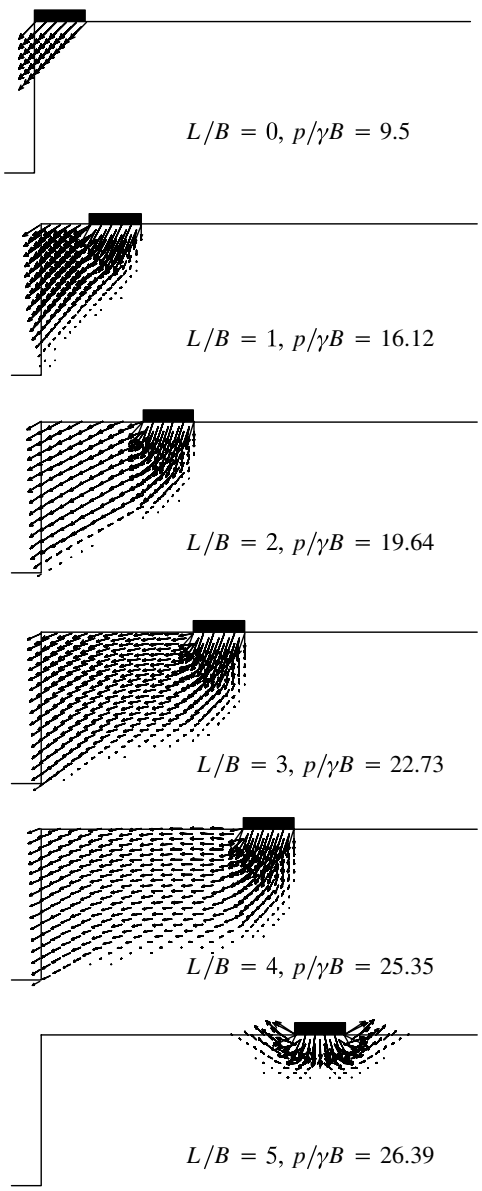

Fig. 16. Velocity diagrams for various L/B (smooth base, $\beta = 90°$, $c_u/\gamma B = 5$)

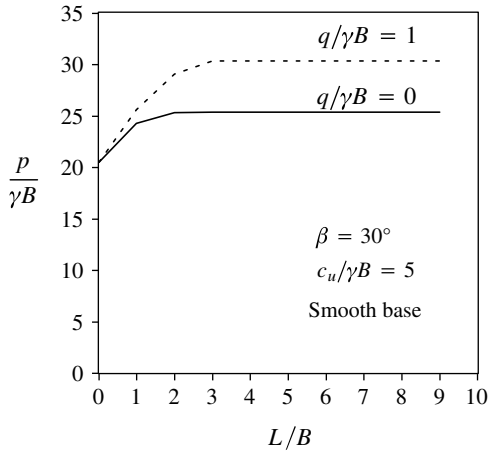

Fig. 17. Effect of $q/\gamma B$ on the bearing capacity for various L/B ($\beta = 30°$, $c_u/\gamma B = 5$)

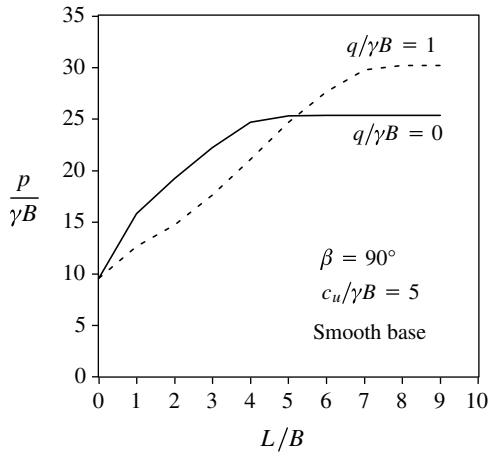

Fig. 18. Effect of $q/\gamma B$ on the bearing capacity for various L/B ($\beta = 90°$, $c_u/\gamma B = 5$)

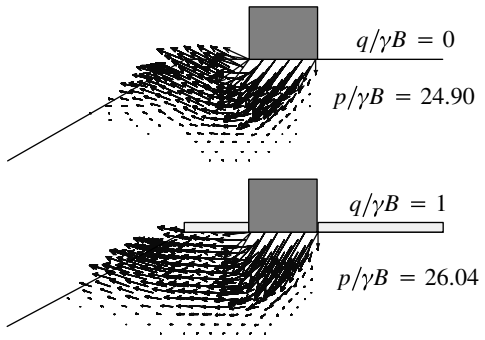

Fig. 19. Comparison of velocity diagrams between various surcharges (smooth base, $\beta = 30°$, $c_u/\gamma B = 5$, $L/B = 1$)

collapse mechanisms at values of $c_u/\gamma B$ located on the linear portion of the curves shown in Figs. 8–11 and checking that they do not extend below the toe of the slope. It was found that all failure mechanisms are essentially unaffected by the toe of the slope when $H/B \geq 3$. For slopes in which $\beta = 90°$ and $L/B = 1$ to 4, the location of the toe was found to affect the collapse load only very slightly (Fig. 16). For these cases, by increasing the value of H/B from 1 to 4 leads to a reduction in the normalized bearing capacity $p/\gamma B$ by less than 1.5%. It can therefore, be concluded that the results herein are applicable for all values of $H/B \geq 3$.

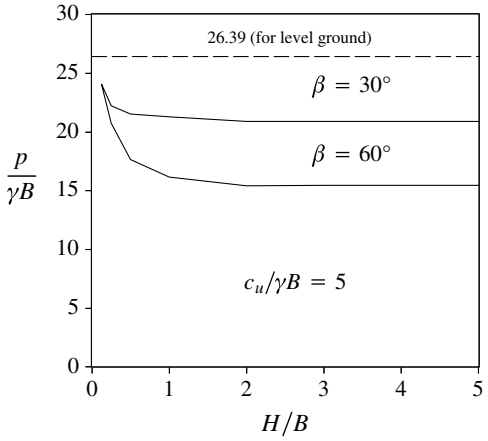

Fig. 20. Effect of H/B (smooth base, $L/B = 0$)

For values of $H/B < 3$, further upper bound analyses were performed to investigate the effect of H/B for a range of slopes and values of L/B. It was found, provided that overall slope failure does not occur, that the normalized bearing capacity $p/\gamma B$ will remain unchanged as H/B is decreased below 3 until reaching a critical value of H/B. This critical value of H/B will be a function of the problem geometry. Fig. 20 presents the results for $\beta = 30°$ and 60°, $L/B = 0$, and $c_u/\gamma B = 5$. At a very small critical value of H/B, there exists a sharp increase in the normalized bearing capacity as the value approaches that for a surface footing with no slope present. Physically, this makes perfect sense. For very small values of H/B, the influence of the slope on the collapse mechanism becomes negligible, and, in fact, the slope becomes part of the bearing capacity mechanism itself. Therefore, it can be concluded that results presented throughout this paper can also be used to estimate the ultimate bearing capacity for problems in which $H/B < 3$; however, the results will be conservative.

Suggested Procedure for Estimation of Bearing Capacity

The following step-by-step procedure is proposed for estimating the ultimate capacity of footings placed near the edge of a purely cohesive slope:

1. Determine representative values of the material parameters c_u, γ, $c_u/\gamma B$, and L/B;
2. Determine value of $(c_u/\gamma B)_{\text{crit}}$ in which full slope failure has occurred

$$(c_u/\gamma B)_{\text{crit}} = N_f \frac{H}{B}$$

   in which $N_f = c_u/\gamma H F_s$ can be obtained from Taylor's charts by putting $F_s = 1.0$;
3. Check that the value of $c_u/\gamma B > (c_u/\gamma B)_{\text{crit.}}$, if $c_u/\gamma B \leq (c_u/\gamma B)_{\text{crit}}$, then overall slope failure has occurred, if $c_u/\gamma B > (c_u/\gamma B)_{\text{crit}}$, then the slope is stable, progress to step 4; and
4. Calculate $p/\gamma B$ by using design charts in Figs. 8–11.

Example of Application

We now illustrate how to use the results presented to determine the ultimate bearing capacity of a footing resting on a slope in clay.

Problem: A smooth strip footing of width 1.0 m is to be placed 1.0 m back from the edge of a 5 m high, 60° slope in a homogeneous clay. Determine the ultimate bearing capacity given the clay has an undrained shear strength of $c_u = 50$ kPa and unit weight $\gamma = 15$ kN/m^3.

1. Given $c_u = 50$ kPa and $\gamma = 15$ kN/m^3, $L/B = 1/1 = 1$.
2. $c_u/\gamma B = 50/15(1) = 3.33$.
3. For a 60° slope, $N_f = 0.196$.
4. Value of $(c_u/\gamma B)_{\text{crit}}$ in which full slope failure has occurred and $p/\gamma B = 0$ will be given by

$$(c_u/\gamma B)_{\text{crit}} = N_f \frac{H}{B} = 0.196(5) = 0.98$$

5. Check that $c_u/\gamma B > (c_u/\gamma B)_{\text{crit}}$, $3.33 > 0.98$ therefore, slope is stable.
6. By using Fig. 9, $p/\gamma B \approx 13.5$, $P = (13.5)(15)(1) = 202.5$ kPa.

The actual average finite element upper and lower bound value for this problem was found to be $P = 203.5$ kPa (+0.5%).

Conclusions

The undrained bearing capacity of a strip footing resting near the edge of a slope has been investigated. By using finite-element limit analysis formulations of the lower and upper bound theorems, rigorous bounds on the bearing capacity of footings on slopes for a wide range of parameters have been calculated. The results obtained have been presented in normalized bearing capacity with respect to the soil unit weight (γ) and the footing width (B). The study indicates that there exists a critical value of strength ratio that separates two types of failure (i.e., bearing capacity failure and slope failure). This critical value of $(c_u/\gamma B)_{\text{crit}}$ is an important parameter in the design of foundations located near slopes. A procedure for estimation of the bearing capacity is suggested, and an example is given.

References

Chen, W. F. (1975). *Limit analysis and soil plasticity*, Elsevier, Amsterdam, Netherlands.

Davis, E. H., and Booker, J. R. (1973). "Some adaptations of classical plasticity theory for soil stability problems." *Proc. Symp. Role of Plasticity in Soil Mechanics*, A. C. Palmer, ed., Cambridge University, Cambridge, UK, 24–41.

de Buhan, P., and Garnier, D. (1994). "Analysis of the bearing capacity reduction of a foundation near a slope by means of the yield design theory." *Revue Française de Géotechnique*, 68, 21–32 (in French).

de Buhan, P., and Garnier, D. (1998). "Three dimensional bearing capacity analysis of a foundation near a slope." *Soils Found.*, 38(3), 153–163.

Drucker, D. C., Greenberg, W., and Prager, W. (1952). "Extended limit design theorems for continuous media.." *Q. Appl. Math.*, 9, 381–389.

Kusakabe, O., Kimura, T., and Yamaguchi, H. (1981). "Bearing capacity of slopes under strip loads on the top surface." *Soils Found.*, 21(4), 29–40.

Krabbenhøft, K., Lyamin, A. V., Hjiaj, M., and Sloan, S. W. (2005). "A new discontinuous upper bound limit analysis formulation." *Int. J. Numer. Methods Eng.*, 63, 1069–1088.

Lyamin, A. V. (1999). "Three-dimensional lower bound limit analysis using nonlinear programming." Ph.D. Thesis, Univ. of Newcastle, Australia.

Lyamin, A. V., and Sloan, S. W. (2002a). "Lower bound limit analysis using non-linear programming." *Int. J. Numer. Methods Eng.*, 55, 573–611.

Lyamin, A. V., and Sloan, S. W. (2002b). "Upper bound limit analysis using linear finite elements and non-linear programming." *Int. J. Numer. Anal. Methods Geomech.*, 26, 181–216.

Meyerhof, G. G. (1957). "The ultimate bearing capacity of foundations on slopes." *Proc., 4th Int. Conf. on Soil Mechanics and Foundation Engineering*, 1, 384–386.

Michalowski, R. L. (1995). "Slope stability analysis: a kinematical approach." *Geotechnique*, 45(2), 283–293.

Narita, K., and Yamaguchi, H. (1990). "Bearing capacity analysis of foundations on slopes by using log-spiral sliding surfaces." *Soils Found.*, 30(3), 144–152.

Shiau, J. S., Lyamin, A. V., and Sloan, S. W. (2003). "Bearing capacity of a sand layer on clay by finite element limit analysis" *Can. Geotech. J.*, 40, 900–915.

Shields, D., Chandler, N., and Garnier, J. (1990). "Bearing capacity of foundations in slopes" *J. Geotech. Eng.*, 116(3), 528–537.

Sloan, S. W. (1988). "Lower bound limit analysis using finite elements and linear programming." *Int. J. Numer. Anal. Methods Geomech.*, 12, 61–67.

Sloan, S. W. (1989). "Upper bound limit analysis using finite elements and linear programming." *Int. J. Numer. Anal. Methods Geomech.*, 13, 263–282.

Sloan, S. W., and Kleeman, P. W. (1995). "Upper bound limit analysis using discontinuous velocity fields." *Comput. Methods Appl. Mech. Eng.*, 127, 293–314.

Sokolovski, V. V. (1960). *Statics of granular media*, Butterworth Scientific Publications, London.

Taylor, D. W. (1937). "Stability of Earth Slopes." *J. Boston Soc. Civ. Eng.*, 24(3), July, 197–247, reprinted in *Contributions to Soil Mechanics 1925-1940*(1940), Boston Society of Civil Engineers, 337–386.